Double-Shelled NiO-NiCo2O4 Heterostructure@Carbon Hollow Nanocages as an Efficient Sulfur Host for Advanced Lithium-Sulfur Batteries

DOI: 10.1002/ ((please add manuscript number))

Article type: ((**Full Paper**))

Double-Shelled NiO-$NiCo_2O_4$ Heterostructure@Carbon Hollow Nanocages as An Efficient Sulfur Host for Advanced Lithium-Sulfur Batteries

Linyu Hu,[†] Chunlong Dai,[†] Heng Liu, Yi Li, Bolei Shen, Yuming Chen, Shu-Juan Bao, and Maowen Xu**

L. Y. Hu, C. L. Dai, H. Liu, Y. Li, B. L. Shen, Prof. S. J. Bao, Prof. M. W. Xu

Institute for Clean Energy & Advanced Materials, Faculty of Materials and Energy, Southwest University, Chongqing 400715, PR China
E-mail: xumaowen@swu.edu.cn

Dr. Y. M. Chen
Department of Nuclear Science and Engineering, Department of Materials Science and Engineering, Massachusetts Institute of Technology, Cambridge, Massachusetts 02139, United State

E-mail: yumingc@mit.edu

Keywords: NiO-$NiCo_2O_4$, heterostructure, double-shelled hollow nanocage, lithium-sulfur batteries, reaction kinetics

Double-shelled NiO-$NiCo_2O_4$ heterostructure@carbon hollow nanocages as an efficient sulfur host have been synthesized to overcome the barriers of lithium-sulfur (Li-S) batteries simultaneously. The double-shelled nanocages can prevent the diffusion of lithium polysulfides (LiPSs) effectively. NiO-$NiCo_2O_4$ heterostructure is able to promote polysulfide conversion reactions. Furthermore, the thin carbon layer outside can improve the electrical conductivity during cycling. Besides, such unique double-shelled hollow nanocage architecture can also accommodate the volumetric effect of sulfur upon cycling. As a result, the prepared S/NiO-$NiCo_2O_4$@carbon (C) electrode exhibits good rate capacities and stable cycling life up to 500 cycles at 0.5 C with a very low capacity decay rate of only ~0.059 % per cycle.

1. Introduction

Li-S batteries, as a promising candidate of next generation energy storage devices for the ever-growing demand, have received widely attentions in terms of their high theoretical energy density and low price and environment benignity of the sulfur cathode.[1] Nevertheless, the commercial application of Li-S batteries is impeded by several obstacles. Primarily, the intrinsic insulating properties of sulfur (5×10^{-30} S cm^{-1}) and the discharged end products inevitably cause the poor utilization of sulfur.[2] Next, there is a significant volume expansion (~ 80%) occurring during the discharge process, leading to the instability of electrode structure.[3] Last but the foremost, the unavoidable dissolution of polysulfides in electrolyte as well as the depressed reaction kinetics of the transformation of polysulfides to Li_2S_2/Li_2S will result in the "shuttle effects".[4]

To tackle aforementioned challenges, intensive efforts have been carried out to design optimized carbon/sulfur cathodes, such as compositing sulfur with mesoporous carbon,[5] carbon nanofibers,[6] carbon nanotubes,[7] carbon spheres[8] and graphene[9]. Although these carbon-based materials greatly improve the electric conductivity of electrode thereby providing high capacities,[10] the weak interaction between nonpolar carbon and polar polysulfides is not sufficient to limit the dissolution of LiPSs. To further boost the polysulfides adsorption capability and promote the redox reaction kinetics, various polar sulfur host, including metal, metal oxides, metal sulfides and perovskite[11-14] are engineered as ideal candidates to not only possess good bonds between polar material and LiPSs, but also accelerate the conversion of LiPSs to solid Li_2S_2/Li_2S, giving rise to a good cycling stability.

Heterostructures constructed from coupling nanocrystals with different band gaps have attracted extensive attentions and widely used in photocatalysis, sensor and energy storage.[15]

Benefiting from the internal electric field at heterointerfaces, heterostructures can facilitate charge transport and enhance the surface reaction kinetics.[16] Inspired by the unique advantages of heterostructures, we propose and construct a double-shelled NiO-$NiCo_2O_4$ heterostructure@C hollow nanocages as an efficeint sulfur host for advanced Li-S batteries. NiO has strong adsorption for LiPSs that can remarkably immobilize LiPSs through physical and chemical interactions at molecular level.[17] However, the low electrical conductivity makes it difficult for the immobilized LiPSs to fully involve in the electrochemical reactions, thus slowing the redox kinetics of LiPSs conversion reactions. Introducting $NiCo_2O_4$ that posseses much better electrical conductivity and higher redox activity into nickel oxides can promote electron transfer for LiPSs conversion reactions.[18]

The synthetic approach to the S/NiO-$NiCo_2O_4$@C composite is schematically shown in **Figure 1**a (for experimental details, see Supporting Information). Uniform Ni-Co prussian blue analogue (PBA) nanocube precursor was first prepared by a facile co-precipitation strategy. Afterwards, double-shelled NiO-$NiCo_2O_4$ heterostructure@C nanocages were obtained through a facile calcination treatment coupled with a simple hydrothermal carbon coating process. After a melt-diffusion process, sulfur was successfully introduced into the NiO-$NiCo_2O_4$ heterostructure@C hollow nanocages. This double-shelled NiO-$NiCo_2O_4$@C hollow nanocage as the sulfur host exhibits multifold features (Figure 1b): i) The hollow structure not only can provide sufficient space for loading sulfur but mitigate volumetric variation of sulfur during cycling; ii) NiO-$NiCo_2O_4$ heterostructure nanocages effectively prevent polysulfide diffusion and accelerate electron transfer for polysulfide conversion reactions, thus remitting the shuttling effect of LiPSs; and iii) The outside carbon layer improves the electrical conductivity for electron transport during cycling. With this

desired design, the S/NiO-$NiCo_2O_4$@C composite manifests considerable specific capacity and remarkable cycle stability.

2. Results and discussion

The Ni-Co PBA nanocube precursors are highly uniform with a rather smooth surface and an average size of 400 nm, as confirmed by field-emission scanning electron microscopy (FESEM) and Transmission electron microscopy (TEM) (see Figure S1a-c). X-ray diffraction (XRD) pattern (see Figure S1d) of the precursor indicates the typical diffraction peaks of $Ni_3[Co(CN)_6]_2$ (JCPDS card NO. 89-3738). After annealed in air at 450 °C, these Ni-Co PBA nanocubes can be convert into Ni-Co mixed oxide nanocages with rough surface, which is composed of NiO (JPCDS card No. 47-1049) and $NiCo_2O_4$ (JPCDS card No. 20-0781) (see Figures S2 and S3). The increase of heating treatment is able to obtain high-crystallinity hollow NiO-$NiCo_2O_4$ heterostructure nanocages (see Figure S4). As depicted in **Figure 2**a and b, the heterostructure nanocages constructed from metal oxdie buliding blocks possess rather rough surface. The size of nanocages is slightly reduced to approximately 300 nm. Besides, the hollow structure of the NiO-$NiCo_2O_4$ nanocage is also observed (Figure 2c). Energy dispersive spectroscopy (EDS) mapping (see Figure S5) indicates the homogenous distribution of Ni, Co and O in the NiO-$NiCo_2O_4$ heterostructure. From the high-magnification TEM image (Figure 2d and e), the NiO-$NiCo_2O_4$ nanocage with a wall thickness of 30 nm is assembled by nanoparticles with a particle size of 10~20 nm. The HRTEM image in Figure 2f shows the lattice fringes of the NiO-$NiCo_2O_4$ heterostructure with *d*-spacing of 0.47 nm and 0.20 nm, corresponding to the (111) and (200) crystal planes of $NiCo_2O_4$ and NiO, respectively. Moreover, the interface between $NiCo_2O_4$ and NiO can be observed clearly, which can act as the highly active sites in both adsorption and electron transfer. Figure S6 shows the Fast Fourier Transforms (FFT) of the NiO-$NiCo_2O_4$ heterostructure

taken from different domains of HRTEM micrograph, further confirming the evidence of the the physical phases of the NiO (Figure S6b), $NiCo_2O_4$ (Figure S6c), and NiO+$NiCo_2O_4$ (Figure S6d), respectively.

Subsequently, a uniform carbon layer derived from glucose is coated onto the surface of NiO-$NiCo_2O_4$ heterostructure nanocages (Figure 2g and h). Meanwhile, the hollow feature of the nanocages can still be well-maintained (Figure 2i-k). The homogeneous distribution of Ni, Co, O and C elements was verified by EDS elemental mapping (see Figure S7). Furthermore, thermogravimetric (TGA) analysis indicates the content of carbon in the NiO-$NiCo_2O_4$ heterostructure@C composite is approximately 20 wt% (see Figure S8). From the magnified TEM image (Figure 2l), it can be found that the thickness of the carbon shell is approximately 10 nm, indicating the successful synthesis of double-shelled NiO-$NiCo_2O_4$ heterostructure@C nanocages. There is no characteristic peaks of carbon (see Figure S9) due to its much lower signal when compared to metal oxside. Raman spectra of the NiO-$NiCo_2O_4$@C shows two broad peaks around 1369 and 1574 cm^{-1} (Figure S10), corresponding to the vibration of carbon atoms with dangling bonds of disordered graphite and the vibration in all sp^2 bonded carbon atoms in a 2-dimensional hexagonal lattice, respectively.[19] Besides, the X-ray photoelectron spectroscopy (XPS) spectrum also confirms the existence of C in the composites (see Figure S11).

The morphology of the materials is well maintained after loading sulfur. Moreover, there is no extra sulfur outside, demonstrating the successful diffusion of sulfur into the nanocages (**Figure 3**a and b). From the XRD pattern (Figure 3c), the peaks between 20- 25° are due to the crystalline sulfur in the S/NiO-$NiCo_2O_4$@C composite. TEM observations (Figure 3d and e) clearly show that the contrast of inner void spaces of the S/NiO-$NiCo_2O_4$@C becomes much darker than that of the NiO-

$NiCo_2O_4$ heterostructure@C nanocage, which reveals the successful accommodation of sulfur into the hollow host. The mass proportion of sulfur in the S/NiO-$NiCo_2O_4$@C composite was determined by TGA as 73 wt% (see Figure 3f). EDS elemental mapping and linear scan of the S/NiO-$NiCo_2O_4$@C composite shows the homogeneous encapsulation of sulfur within the host (Figure 3g and h), proving that sulfur has been infused into the inner part of the NiO-$NiCo_2O_4$ heterostructure@C host.

The electrochemical properties of the S/NiO-$NiCo_2O_4$@C composite is evaluated as the cathode for Li-S batteries. **Figure 4**a shows the cyclic voltammetric (CV) curves of the S-NiO-$NiCo_2O_4$@C electrode for the first 3 cycles. During the cathodic scanning, two stabilized reduction peaks located at 2.27 and 2.04 V correspond to the transformation of sulfur (S_8) to long-chain lithium polysulfides and the conversation of long-chain lithium polysulfides to short-chain lithium polysulfides (Li_2S_2/Li_2S).[20] Figure 4b shows the galvanostatic charge-discharge voltage profiles at various current densities from 0.2 to 2 C. Two typical discharge plateaus and one charge plateau are obvious even at 2 C, indicating a low polarization. Rate capability of the S/NiO-$NiCo_2O_4$@C cathode is shown in Figure 4c. The cathode delivers discharge capacities of 1063.2, 920, 821.7 and 697.9 mAh g^{-1} at the current densities of 0.2, 0.5, 1 and 2 C, respectively. When the current density recovered to 0.2 C, the capacity can be almost maintained, indicating the excellent stability of the structure of the S/NiO-$NiCo_2O_4$@C composite. It is worth mentioning that the NiO-$NiCo_2O_4$@C nanocages cannot contribute to the capacity under the same conditions, as displayed in Figure S12.

The long-term cycling performance (Figure 4d) was evaluated at 0.5 C to confirm the stability of the S/NiO-$NiCo_2O_4$@C cathode. After 500 cycles, a high capacity of 716.9 mAh g^{-1} with high coulombic efficiency of over 98 % can still be maintained. Meanwhile, a low capacity fading of 0.059 % per cycle was obtained. This performance is superior to that of many other metal oxides

electrodes (Figure S22). As a contrast, the S/carbon black (S/CB) cathode displays a comparatively low initial capacity of 690 mAh g^{-1} and suffers rapid capacity decay in the following cycles. Electrochemical impedance spectra (EIS) anlysis of the S/NiO-$NiCo_2O_4$@C electrode in Figure S13 shows that the charge-transfer resistance decreases clearly after cycling, which can be attributed to the activation process. Besides, the low charge-transfer resistances indicate that the irreversible deposition of insoluble reduction products on the surface of the S/NiO-$NiCo_2O_4$@C electrode is very limited. The electric conductivity of NiO-$NiCo_2O_4$@C is about 0.1 S cm^{-1} using four-point probe operation.

In order to further show the superiority of the heterostructure, we also prepared NiO@C and $NiCo_2O_4$@C nanocage hosts and studied their electrochemical performance. As shown in Figures S14 and S15, both the NiO@C and $NiCo_2O_4$@C nanocages show an average size of 300 nm, which are similar to that of the NiO-$NiCo_2O_4$@C nanocages. XRD patterns of the samples show the characteristic diffraction peaks of NiO and $NiCo_2O_4$. The contents of sulfur in the S/NiO@C and S/$NiCo_2O_4$@C composites are ~ 72 wt% and 73 wt%, respectively. Both the S/NiO@C and S/$NiCo_2O_4$@C composites deliver lower capacities at 0.2, 0.5, 1 and 2 C when compared to the S/NiO-$NiCo_2O_4$@C composite (Figure S16). Moreover, they also suffer faster capacity decay. These results indicate the unique advantages of heterostructure we prepared. In addition, the carbonization process for the prepared samples is able to improve the electrochemical performance of the electrodes. Howover, high heating treatment can reudce the samples to from some Ni particles and destory the morphology of hollow structure, which will greatly decrease the electrochemcial performance of the electrodes (Figures S17-S19). To further verify the NiO-$NiCo_2O_4$ heterostructure can effectively restrict the diffusion of LiPSs from the electrode, lithium metal foils

disassembled from different coin cells were compared by FESEM and EDS analysis, as displayed in Figure 4e and Figure S20. The lithium foil from the S/NiO-$NiCo_2O_4$@C cell almost maintains its original morphology, and low intensity signals of sulfur can be observed from elemental mapping and EDS spectrum, suggesting the excellent absorption ability of the NiO-$NiCo_2O_4$ for LiPSs. For the S/CB cell, lithium metal foil shows a looser and rougher surface, indicating a serious shuttle of lithium polysulfides in the cell. In addtion, the shape and structural of the S/NiO-$NiCo_2O_4$@C can be well retained after 500 cycles (Figures 4f and g). Meanwhile, the separator from the S/NiO-$NiCo_2O_4$@C cell shows less color than that from the S/CB cell, further confirming that the NiO-$NiCo_2O_4$ heterostructure effectively restricts lithium polysulfides dissolution upon cycling (Figure 4h).

Polysulfide adsorption measurement, UV–Vis absorption test and XPS measurement were performed to further verify the absorption ability of NiO-$NiCo_2O_4$. As elucidated in **Figure 5**a, the color of the LiPSs solution is basically unchanged after the addition of CB. In contrast, the LiPSs solution changes from brown to colorless after adding NiO-$NiCo_2O_4$. Figure 5b shows the concentration change of Li_2S_4 after the addition of CB and NiO-$NiCo_2O_4$, the peak at 420 nm is linked to S_4^{2-} species.[21] The absorbance intensity of Li_2S_4 solution with NiO-$NiCo_2O_4$ is much weaker than that of Li_2S_4 solution with CB. These findings indicate the strong interaction between LiPSs and NiO-$NiCo_2O_4$. Figure 5c displays the Ni $2p_{3/2}$ XPS spectra comparison of the initial and cycled NiO-$NiCo_2O_4$. The Ni $2p_{3/2}$ XPS spectrum of the initial NiO-$NiCo_2O_4$ exhibits a spin-orbit doublet at 855.6 and 853.7 eV, corresponding to Ni^{3+} and Ni^{2+}, respectively. After cycling, the peaks of Ni^{3+} and Ni^{2+} shift to 856.2 and 854.3 eV, respectively. Figure 5d shows the Co $2p_{3/2}$ spectrum comparison of the initial and cycled NiO-$NiCo_2O_4$. Before cycling, the peaks of Co $2p_{3/2}$ spectrum locate at 781 and 779 eV.[22] After cycling, the peaks of Co $2p_{3/2}$ spectrum shift to 781.4 and 779.5 eV, respectively. The results are in

good agreement with the others.[23] The peak position variation of Ni $2p_{3/2}$ and Co $2p_{3/2}$ spectrums can be attributed to the electron transfer between Li_2S_x and Ni/Co atoms,[13c,24] manifesting the strong chemical interaction between the NiO-$NiCo_2O_4$ and LiPSs.

A combination of CV and galvanostatic discharge-charge tests were carried out to investigate the catalytic effect of the NiO-$NiCo_2O_4$ heterostructure on LiPSs redox reactions. As shown in Figure 5e and Figure S21a, two deformed and widened cathodic peaks of pure S electrode locate at 2.18 and 1.91 V and the anodic peak at 2.56 V. For the NiO-$NiCo_2O_4$+S electrode, two sharp cathodic peaks at 2.29 and 2.0 V and the anodic peak at 2.39 V can be oberved, indicating that NiO-$NiCo_2O_4$ can significantly suppress the electrochemical polarization. The analysis of the onset potentials provides further evidence that the NiO-$NiCo_2O_4$ heterostructure accelerates the redox processes (Figure S21b). Compared with pure S electrode, the NiO-$NiCo_2O_4$+S electrode shows higher onset potentials of cathodic peaks (2.4 and 2.1 V) and a lower anodic peak (2.2 V). Figure 5f shows discharge/charge voltage profiles of pure S and the NiO-$NiCo_2O_4$+S electrode at 0.1 C. The NiO-$NiCo_2O_4$+S electrode shows a discharge capacity of 950.4 mAh g^{-1}, which is much larger than that of the pure S electrode. Furthermore, when compared to pure S electrode the NiO-$NiCo_2O_4$+S electrode possesses a relatively lower polarization value of 179 mV. Both the improved discharge capacity and reductive polarization show that the NiO-$NiCo_2O_4$ heterostructure is able to boost the electrochemical reaction kinetics during cycling.

3. Conclusion

In summary, we propose and design an efficient double-shelled sulfur host in which hollow NiO-$NiCo_2O_4$ heterostructure nanocages are coated by a thin carbon layer. The NiO-$NiCo_2O_4$ heterostructure can efficiently confine LiPSs due to the polar chemisorptive capability, and promote

electron transfer for polysulfide transform into Li_2S_2/Li_2S. This unque structure can maximize the sulfur loading and provide enough space for accommodating the volumetric effect of sulfur upon cycling. Benefiting from the structural and compositional superiorities, the S/NiO-$NiCo_2O_4$@C composite cathode delivers a high specific capacity and a low capacity fading of 0.059 % per cycle over 500 cycles. We believe that our present work would offer effective ideas in fabricating various electrode materials with excellent electrochemical properties for Li-S batteries.

Supporting Information

Supporting Information is available from the Wiley Online Library or from the author.

Acknowledgements

This work is financially supported by grants from the National Natural Science Foundation of China (No. 21773188) and Fundamental Research Funds for the Central Universities (XDJK2017B048).

Linyu Hu and Chunlong Dai contributed equally to this work.

Received: ((will be filled in by the editorial staff))
Revised: ((will be filled in by the editorial staff))
Published online: ((will be filled in by the editorial staff))

References

[1] a) X. Liang, Y. Rangom, C. Y. Kwok, Q. Pang, L. F. Nazar, *Adv. Mater.* **2017**, *29*, 1603040; b) D. Liu, C. Zhang, G. Zhou, W. Lv, G. Ling, L. Zhi, Q. H. Yang, *Adv. Sci.* **2017**, *5*, 1700270.

[2] Z. Liang, G. Zheng, W. Li, Z. W. Seh, H. Yao, K. Yan, D. Kong, Y. Cui, *ACS Nano* **2014**, *8*, 5249-5256.

[3] a) P. Xiao, F. Bu, G. Yang, Y. Zhang, Y. Xu, *Adv. Mater.* **2017**, *29*, 1703324; b) L. Y. Hu, C. L. Dai, J. M. Lim, Y. M. Chen, X. Lian, M. Q. Wang, Y. Li, P. H. Xiao, G. Henkelman, M. W. Xu, *Chem. Sci.* **2018**, *9*, 666-675.

[4] a) H. J. Peng, G. Zhang, X. Chen, Z. W. Zhang, W. T. Xu, J. Q. Huang, Q. Zhang, *Angew. Chem.* **2016**, *128*, 1-6; b) C. Dai, L. Hu, M. Q. Wang, Y. Chen, J. Han, J. Jiang, Y. Zhang, B. Shen, Y. Niu, S. J. Bao, M. Xu, *Energy Storage Mater.* **2017**, *8*, 202-208.

[5] a) J. Schuster, G. He, B. Mandlmeier, T. Yim, K. T. Lee, T. Bein, L. F. Nazar, *Angew. Chem. Int. Ed.* **2012**, *51*, 3591-3595; b) L. Sun, D. Wang, Y. Luo, K. Wang, W. Kong, Y. Wu, L. Zhang, K. Jiang, Q. Li, Y. Zhang, J. Wang, S. Fan, *ACS Nano* **2015**, *10*, 1300-1308.

[6] a) Q. Li, Z. Zhang, Z. Guo, Y. Lai, K. Zhang, J. Li, *Carbon* **2014**, *78*, 1-9; b) X. Song, S. Q. Wang, Y. Bao, G. X. Liu, W. P. Sun, L. X. Ding, H. K. Liu, H. H. Wang, *J. Mater. Chem. A* **2017**, *5*, 6832-6839.

[7] X. B. Cheng, J. Q. Huang, Q. Zhang, H. J. Peng, M. Q. Zhao, F. Wei, *Nano Energy* **2014**, *4*, 65-72.

[8] F. Xu, Z. W. Tang, S. Q. Huang, L. Y. Chen, Y. R. Liang, W. C. Mai, H. Zhong, R. W. Fu, D. C. Wu, *Nat. Commun.* **2015**, *6*, 7221.

[9] a) H. Wang, Y. Yang, Y. Liang, J. T. Robinson, Y. Li, A. Jackson, Y. Cui, H. Dai, *Nano Lett.* **2011**, *11*, 2644-2647; b) G. Zhou, L. C. Yin, D. W. Wang, L. Li, S. Pei, I. R. Gentle, F. Li, H. M. Cheng, *ACS Nano* **2013**, *7*, 5367-5375.

[10] L. Xia, S. Q. Wang, G. X. Liu, L. X. Ding, D. D. Li, H. H. Wang, S. Z. Qiao, *small* **2016**, *12,* 853-859;

[11] a) M. D. Zhang, C. Yu, C. T. Zhao, X. D. Song, X. T. Han, S. H. Liu, C. Hao, J. S. Qiu, *Energy Storage Mater.* **2016**, *5*, 223-229; b) S. H. Liu, J. Li, X. Yan, Q. F. Su, Y. H. Lu, J. S. Qiu, Z. Y. Wang, X. D. Lin, J. L. Huang, R. L. Liu, B. N. Zheng, L. Y. Chen, R. W. Fu, D. C. Wu, *Adv. Mater.* **2018**, 1706895. DOI: 10.1002/adma.201706895.

[12] a) Z. Li, J. Zhang, B. Guan, D. Wang, L. M. Liu, X. W. Lou, *Nat. Commun.* **2016**, *7*, 13065; b) X. Wang, T. Gao, X. Fan, F. Han, Y. Wu, Z. Zhang, J. Li, C. Wang, Adv. Funct. Mater. **2016**, *26*, 7164-7169; c) W. Xue, Q. B. Yan, G. Xu, L. Suo, Y. Chen, C Wang, C. Wang, J. Li, *Nano Energy* **2017**, *38*, 12-18.

[13] a) Y. Lu, X. N. Li, J. W. Liang, L. Hu, Y. C. Zhu, Y. T. Qian, *Nanoscale,* **2016**, *8*, 4733-4741; b) T. Y. Lei, W. Chen, J. W. Huang, C. Y. Yan, H. X. Sun, C. Wang, W. L. Zhang, Y. R. Li, J. Xiong, *Adv. Energy Mater.* **2016**, 7, 1601843. c) C. Dai, J-M Lim, M. Wang, L. Hu, Y. Chen, Z. Chen, H. Chen, S. J. Bao, B. Shen, Y. Li, G. Henkelman, M. Xu, *Adv. Funct. Mater.* **2018**, *28*, 1704443; d) C. Ye, L. Zhang, C. X. Guo, D. D. Li, A. Vasileff, H. H. Wang, S. Z. Qiao, *Adv. Funct. Mater.* **2017**, 27, 1702524.

[14] L. Kong, X. Chen, B. Q. Li, H. J. Peng, J. Q. Huang, J. Xie, Q. Zhang, *Adv. Mater.* **2017**, *30*, 1705219.

[15] a) L. Huang, F. Peng, H. Wang, H. Yu, Z. Li, *Catal. Commun.* **2009**, *10*, 1839-1843; b) D. Zhai, B. Liu, Y. Shi, L. Pan, Y. Wang, W. Li, R. Zhang, G. Yu, *ACS Nano* **2013**, *7*, 3540-3546; c) T. Zhou, W. Lv, J. Li, G. Zhou, Y. Zhao, S. Fan, B. Liu, B. Li, F. Kang, Q. H. Yang, *Energy Environ. Sci.* **2017**, *10*, 1694-1703; d) W. Zhou, C. Cheng, J. Liu, Y. Y. Tay, J. Jiang, X. Jia, J. Zhang, H. Gong, H. H. Hng, T. Yu, H. J. Fan, *Adv. Funct. Mater.* **2011**, *21*, 2439-2445.

[16] Y. Zheng, T. F. Zhou, C. Zhang, J. Mao, H. Liu, Z. Guo, *Angew. Chem. Int. Ed.* **2016**, *55*, 3408-3413.

[17] J. Zheng, J. Tian, D. Wu, M. Gu, W. Xu, C. Wang, F. Gao, M. H. Engelhard, J. G. Zhang, J. Liu, J. Xiao, *Nano Lett.* **2014**, *14*, 2345-235.

[18] a) L. Yu, G. Zhang, C. Z. Yuan, X. W. Lou, *Chem. Commun.,* **2013**, *49*, 137-139; b) J. Li, S. Xiong, Y. Liu, Z. Ju, Y. Qian, *ACS Appl. Mater. Interfaces* **2013**, *5*, 981-988.

[19] a) H. S. Qian, S. H. Yu, L. B. Luo, J. Y. Gong, L. F. Fei, X. M. Liu, *Chem. Mater.,* **2006**, *18,* 2102-2108; b) Y. H. Ni, L. Jin, L. Zhang, J. M. Hong, *J. Mater. Chem.* **2010**, *20*, 6430-6436; c) Y. Qi, N. Du, H. Zhang, P. Wu, D. Yang, *J. Power Sources* **2011***, 196,* 10234-10239.

[20] a) X. Wang, G. Li, J. Li, Y. Zhang, A. Wook, A. Yu, Z. Chen, *Energy Environ. Sci.* **2016**, *9*, 2533-2538; b) L. Li, L. Chen, S. Mukherjee, J. Gao, H. Sun, Z. Liu, X. Ma, T. Gupta, C. V. Singh, W. Ren, H. M. Cheng, N. Koratkar, *Adv. Mater.* **2017**, *29*, 1602734.

[21] Z. Xiao, Z. Yang, L. Wang, H. Nie, M. Zhong, Q. Lai, X. Xu, L. Zhang and S. Huang, *Adv. Mater.* **2015**, *27*, 2891-2898.

[22] A. Sivanantham, P. Ganesan, S. Shanmugam, *Adv. Funct. Mater.* **2016**, *26*, 4661-4672.

[23] a) J. Pu, Z. H. Shen, J. X. Zheng, W. L. Wu, C. Zhu, Q. W. Zhou, H. G. Zhang, F. Pan, *Nano Energy* **2017**, *37*, 7-14; b) C. X. Li, S. H. Dong, D. X. Guo, Z. W. Zhang, M. Q. Wang, L. W. Yin, *Electrochimica Acta* **2017**, *251*, 43-50.

[24] a) Q. Pang, D. Kundu, L. F. Nazar, *Mater. Horiz.* **2016**, *3*, 130-136; b) Z. Chang, H. Dou, B. Ding, J. Wang, Y. Wang, X. D. Hao, D. R. MacFarlane, *J. Mater. Chem. A* **2017**, *5*, 250-257; c) Z. Yuan, H. J. Peng, T. Z. Hou, J. Q. Huang, C. M. Chen, D. W. Wang, X. B. Cheng, F. Wei, Q. Zhang, *Nano Lett.* **2016**, *16*, 519-527.

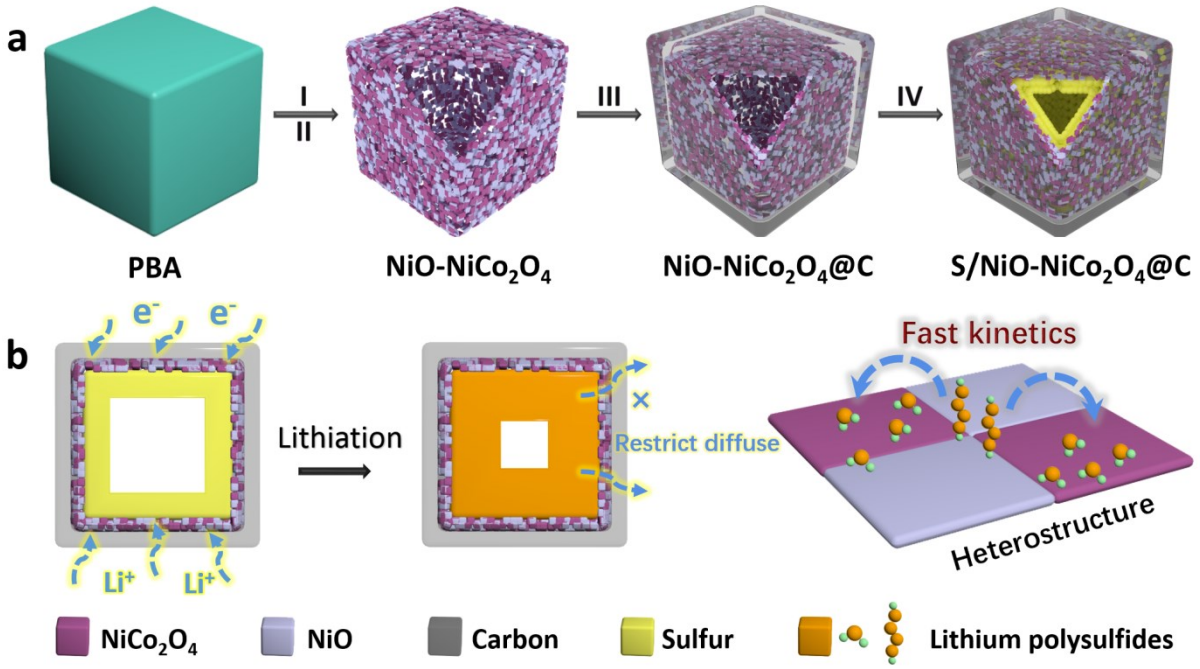

Figure 1. Illustration of the a) synthesis and b) advantages of the S/NiO-$NiCo_2O_4$@C composite.

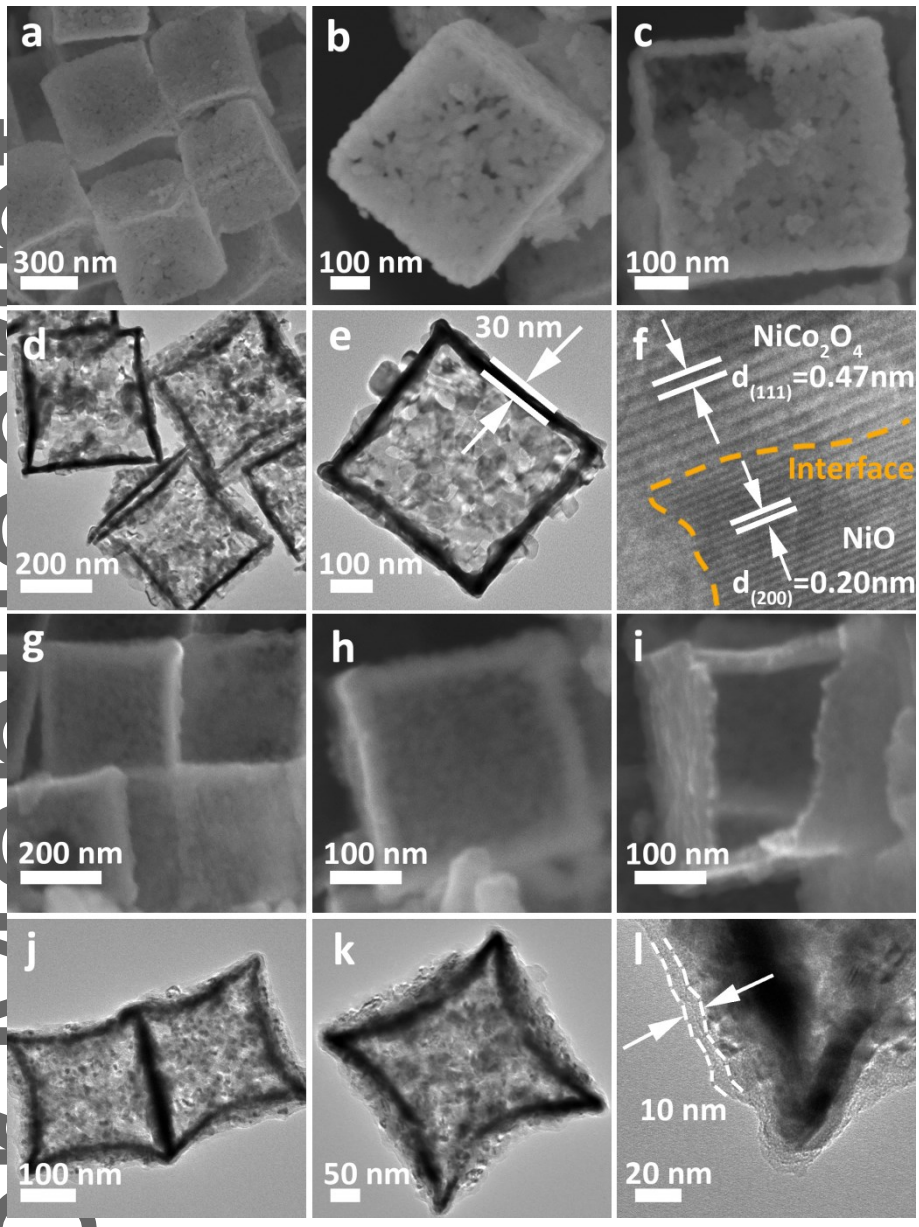

Figure 2. Characterization of NiO-$NiCo_2O_4$ heterostructure and NiO-$NiCo_2O_4$ heterostructure@C hollow nanocages. a-c) FESEM, d,e) TEM, and f) HRTEM images of the NiO-$NiCo_2O_4$ heterostructure hollow nanocages. g-i) FESEM and j-l) TEM images of the double-shelled NiO-$NiCo_2O_4$ heterostructure@C hollow nanocages.

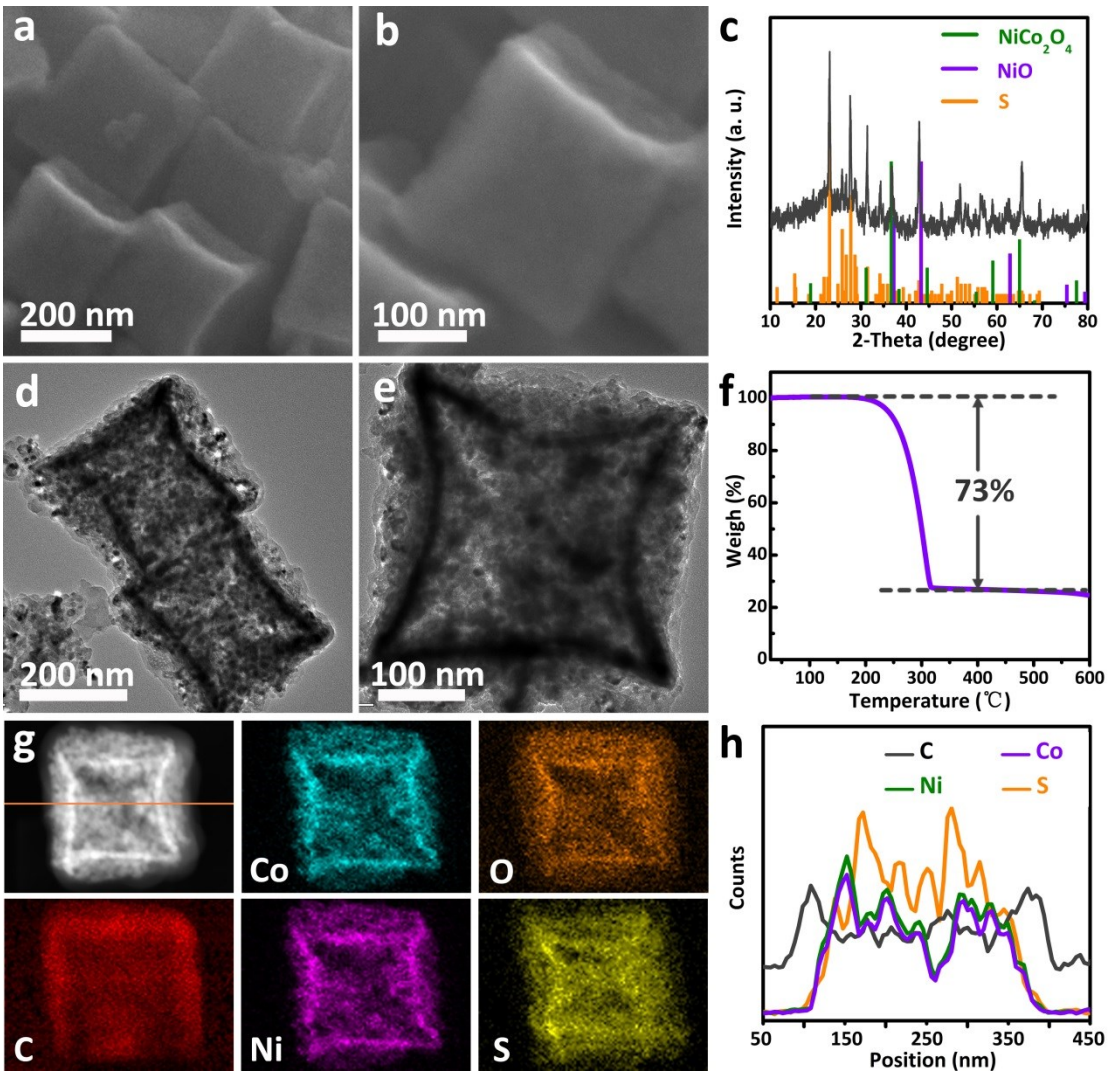

Figure 3. Characterization of S/NiO-$NiCo_2O_4$@C composite. a,b) FESEM images, c) XRD pattern, d,e) TEM images, f) TGA curve, g) EDS elemental mappings and h) linear elemental distributions of the S/NiO-$NiCo_2O_4$@C composite.

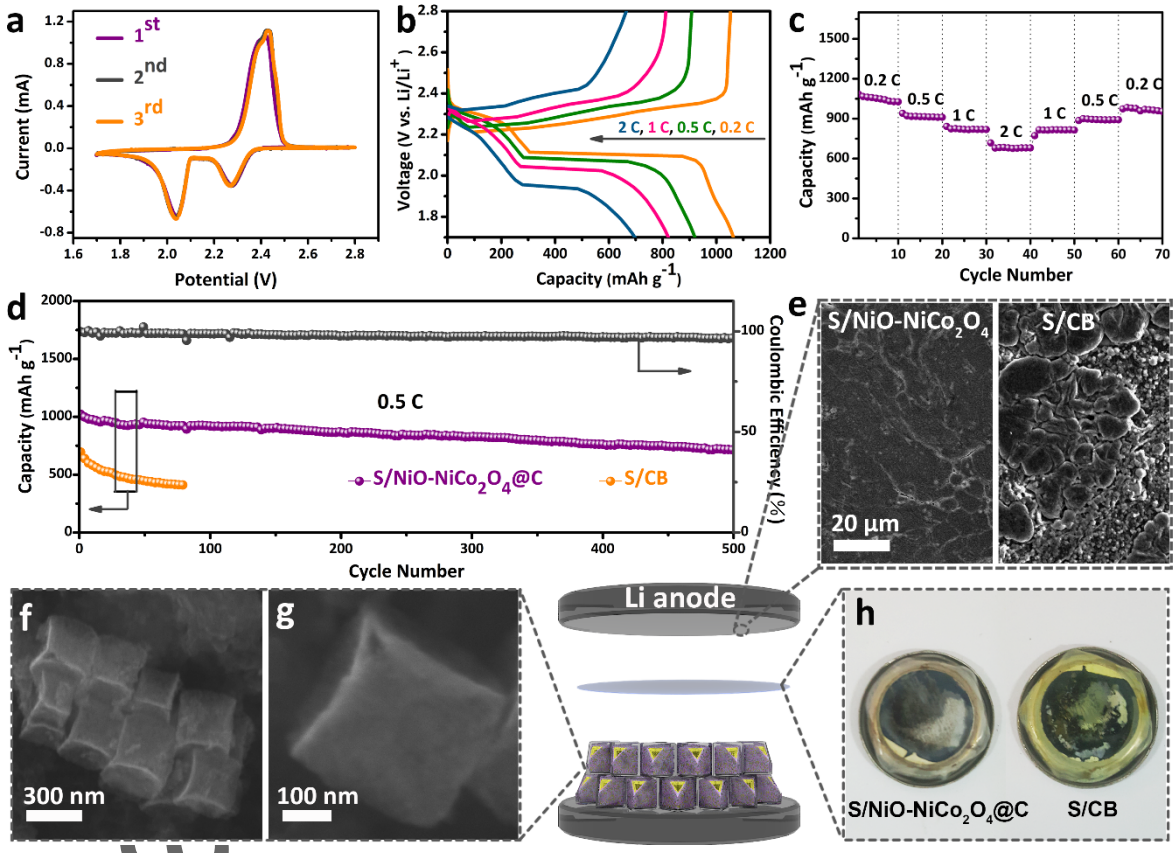

Figure 4. Electrochemical performance of the S/NiO-$NiCo_2O_4$@C composite. a) CV curves at a scan rate of 0.1 mV s^{-1}. b) Voltage profiles and c) Rate capacities at various current densities from 0.2 to 2 C. d) Prolonged cycling performance at 0.5 C. e) FESEM images of lithium metal form the S/NiO-$NiCo_2O_4$@C and S/CB electrodes. f, g) FESEM images of the S/NiO-$NiCo_2O_4$@C composite after cycling. h) The separators of the S/CB and S/NiO-$NiCo_2O_4$@C composite after cycling.

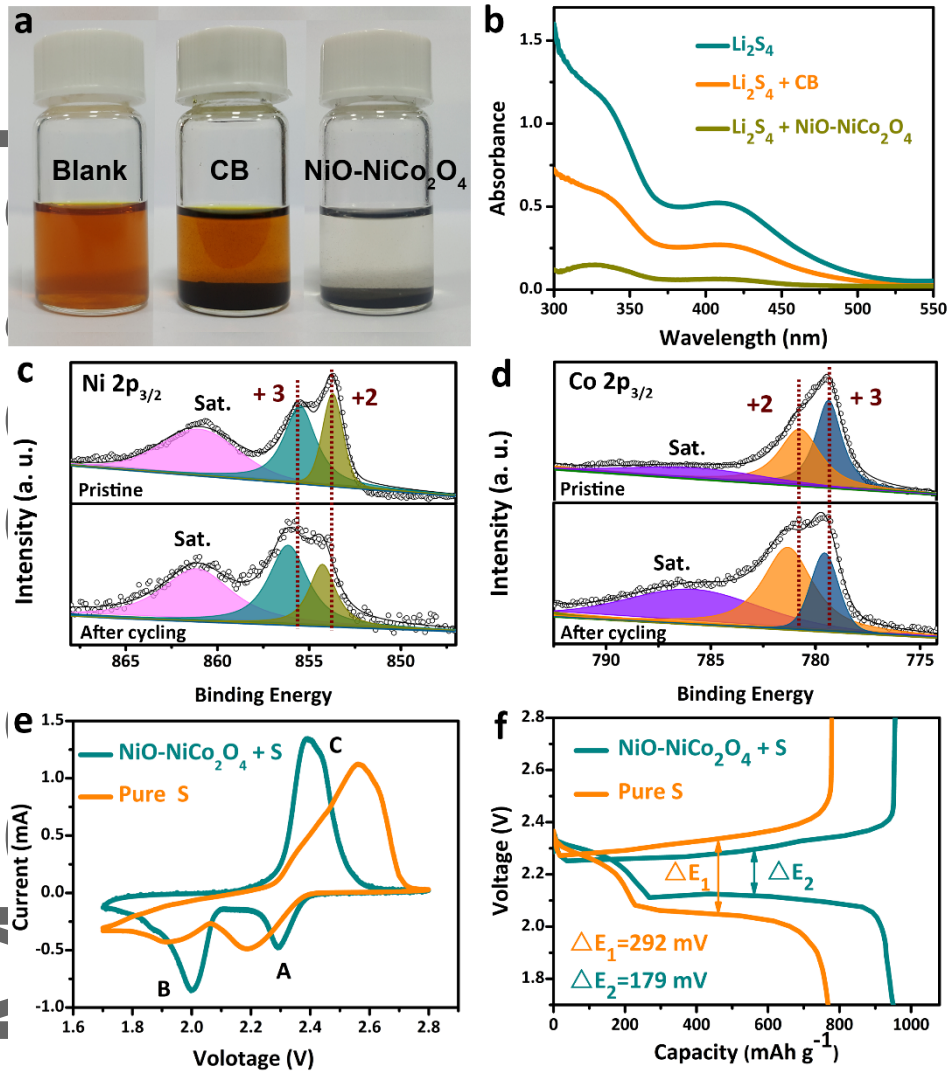

Figure 5. The strong absorption ability and the improved electrochemical reaction kinetics of NiO-$NiCo_2O_4$. a) Polysulfide entrapment by the CB and NiO-$NiCo_2O_4$ heterostructure nanocages. b) UV–Vis absorption spectra of Li_2S_4 solution before and after adding CB or NiO-$NiCo_2O_4$. The comparison of High-resolution XPS spectra of c) Ni $2p_{3/2}$ and d) Co $2p_{3/2}$ of the NiO-$NiCo_2O_4$ before and after cycling. e) CV curves and f) discharge–charge curves of the pure S and NiO-$NiCo_2O_4$ + S electrodes.

An efficient double-shelled hollow sulfur host in which hollow NiO-$NiCo_2O_4$ heterostructure nanocages constructed from building blocks of NiO-$NiCo_2O_4$ nanoparticles are sealed by a thin carbon layer has been proposed and designed. Benefiting from the structural and compositional advantages, the S/NiO-$NiCo_2O_4$ @C composite cathode shows excellent electrochemical performance.

Keyword: NiO-$NiCo_2O_4$, heterostructure, double-shelled hollow nanocage, lithium-sulfur batteries, reaction kinetics

Linyu Hu,[†] Chunlong Dai,[†] Heng Liu, Yi Li, Bolei Shen, Yuming Chen,* Shu-Juan Bao, and Maowen Xu*

Double-Shelled NiO-$NiCo_2O_4$ Heterostructure@Carbon Hollow Nanocages as An Efficient Sulfur Host for Advanced Lithium-Sulfur Batteries

ToC figure